

Estimating Beverly Hills Xeriscaping Water Savings with NAIP-derived NDVI

Aaron Goodman

UCLA GEOG 411 Fall 2024

Abstract: *This study uses archive National Agricultural Imagery Program (NAIP) data to investigate the reduction of vegetation in the city of Beverly Hills, as a proxy to estimate the city's water savings between 2009 and 2020 as a result of widespread Xeriscaping. By using the evapotranspiration (ET) method outlined by the U.S. Department of Energy's Federal Energy Management Program, this study aims to estimate Beverly Hills' water savings in gallons per year by sourcing "Irrigation Area" estimates from a data-driven interpretation of Normalized Difference Vegetation Index (NDVI) results for 2020, 2016, and 2009. Discussion of the rate of change of Irrigation Area also provides insight into the timeline of Xeriscaping adoption across the city.*

I. Problem Statement

Water conservation has long been a consideration in urban development, especially as the acceleration of climate change introduces drought conditions in regions around the American Southwest, which vary in their levels of mitigating infrastructure. For Greater Los Angeles in particular, the tenuous nature of the region's water supply makes for greater pressure to utilize limited freshwater strategically (Kahrl 1982). This pressure increased towards the end of the 2000's when, on October 5, 2009, President Obama's Executive Order 13514 required Federal agencies to reduce and develop a baseline for industrial, landscaping, and agricultural water

consumption; specifically, EO 13514 required a 2% annual reduction in water use through fiscal year 2020 (U.S. Department of Energy 2010).

One popular method by which cities and residents can reduce water consumption is through Xeriscaping, which involves the replacement of water-hungry vegetation with native plants, or non-native plants that are more suited to arid, drought-like conditions (Saher, et al. 2022). This shifts both total vegetation cover, as well as type, and has been proven to reduce required irrigation costs considerably in various regions (Ismaeil & Sobaih 2022). As the deadline for EO 13514's 2% annual reduction in water use has long passed, this study sets out to assess the city of Beverly Hills's success in reducing water use via Xeriscaping or vegetation reduction.

II. Introduction

To investigate the change in Beverly Hills' water use over the course of the examined time period (2009 – 2020), this study will use aerial imagery from the National Agricultural Imagery Program (NAIP), and the Normalized Difference Vegetation Index (NDVI), to highlight shifts in the make up of the city's land cover. The selection of these data and methods draws from frameworks set forth by the United States Department of Energy's Federal Energy Management Program (U.S. Department of Energy 2010), as well as from extant literature which examine water use and climate health through remotely sensed multispectral imagery (Li, et al. 2009; Bhattarai & Wagle 2022).

The structure of this report follows: Section III includes a literature review of relevant journal articles which informed my methods of data analysis and interpretation. Section IV lists important details regarding the selected NAIP imagery, and the processing operations required to be able to use them for visualization and analysis. Section V provides a concise summary of

results from calculations like NDVI and Δ NDVI for the sampled years. Section VI provides a more detailed discussion of these results, and identifies potential sources of error and uncertainty. Section VII concludes the report with a brief assessment of Beverly Hills' success in water use reduction.

III. Background (Literature Review)

The greatest contributor to the development of this study's methods is the framework set forth by the U.S. D.o.E.'s "Guidelines for Estimating Unmetered Landscaping Water Use." This document, and its illustration of water use estimation by means of the evapotranspiration (ET) method, provides a rough plan with which this study can approach evaluation of Beverly Hills' annual water savings in gallons per year with limited expertise (U.S. Department of Energy 2010).

The simplicity of D.o.E.'s water use estimation model contrasts more rigorous models of evapotranspiration demonstrated in studies driven by remotely sensed imagery (Li, et al. 2009; Bhattarai & Wagle 2021). Beyond evapotranspiration, remote sensing literature also demonstrates other methods by which researchers can evaluate water savings and urban heat according to satellite or aerial imagery (Ismaeil & Sobaih 202022; Stephen 2018).

Scholarly stances vary regarding the observable benefits and drawbacks of Xeriscaping as one means of water savings. While it has been proven that Xeriscaping can facilitate a considerable reduction in irrigation requirements for variety of landscapes, the elimination of vegetation like turf can result in increased urban heat as well (Saher, et al. 2022; Winseck 2023).

IV. Data and Methods

I selected historical National Agricultural Imagery Program (NAIP) data for analysis because of its fine spatial resolution, which is far higher than that of the Landsat 5 TM and Landsat 8

OLI. Small image pixels proved essential to this investigation because of the small size of Beverly Hills. However, one drawback of working with archive NAIP imagery is the collection's lower temporal resolution when compared to imagery collections like that of Landsat. Had this investigation been carried out with Landsat imagery, access to scenes from the same time of the summer every year (i.e. scenes with consistent solar angles) would ensure greater certainty in spectral analysis. Nonetheless, I felt that the benefits of the NAIP imagery's high spatial resolution outweighed the drawback of its inconsistent solar angles.

The full extent of Beverly Hills is captured in four separate NAIP images. I sampled each of these four tiles for three calendar years. I chose either end, and a rough midpoint, of the timeframe of interest: 2020, 2016, and 2009. For 2009, I was able to find 4-band multispectral images for all four tiles that were captured on the same day. Unfortunately, the multispectral imagery I found for 2016 and 2020 included two tiles taken on one day, and two tiles taken one or more days later. The image names follow:

*m_3411861_ne_11_060_20200515; m_3411861_se_11_060_20200515
m_3411862_nw_11_060_20200505; m_3411862_sw_11_060_20200505
m_3411861_ne_11_060_20160711; m_3411861_se_11_060_20160711
m_3411862_nw_11_060_20160710; m_3411862_sw_11_060_20160710
m_3411861_ne_11_060_20090626; m_3411861_se_11_060_20090626
m_3411862_nw_11_060_20090626; m_3411862_sw_11_060_20090626*

Notable pre-processing steps were required before NDVI and Δ NDVI analysis. In particular, the four image tiles from a given year had to be normalized to a reference image selected from that year, before the tiles could be accurately “mosaicked” into one raster for NDVI calculation. Additionally, this process had to be repeated independently for all relevant image bands—in my case, Band 4: NIR and Band 1: Red (for NDVI calculation and Color Infrared visualization), and

Band 2: Green (for Color Infrared visualization). I normalized 4 tiles * 3 bands * 3 years = 36 images according to the following formula:

$$\frac{(band_{tile} - mean(band_{ref.tile}))}{sd(band_{ref.tile})}$$

Table 1 below shows statistics (minimum, maximum, mean value, standard deviation) for each relevant band of the reference tile selected for each year:

Table 1: Statistics by Image Band for selected "Reference Tiles", 2020, 2016, 2009

Reference Tile	Band	Band Color	Min	Max	Mean	Std. Dev.
<i>m_3411861_se_11_060_20200515</i>	B1	Red	17	221	114.0252	40.90038
<i>m_3411861_se_11_060_20200515</i>	B2	Green	28	213	115.062	34.54023
<i>m_3411861_se_11_060_20200515</i>	B4	NIR	2	227	117.2329	38.19406
<i>m_3411862_sw_11_h_20160710</i>	B1	Red	24	240	112.3385	43.55939
<i>m_3411862_sw_11_h_20160710</i>	B2	Green	25	235	109.8254	40.08312
<i>m_3411862_sw_11_h_20160710</i>	B4	NIR	34	247	115.409	35.8944
<i>m_3411862_sw_11_1_20090626</i>	B1	Red	59	255	157.9207	49.88834
<i>m_3411862_sw_11_1_20090626</i>	B2	Green	60	255	157.0373	46.61486
<i>m_3411862_sw_11_1_20090626</i>	B4	NIR	53	255	157.8778	41.24585

After 36 unique image normalization calculations, the four tiles from each sampled year were mosaicked into one single-band raster image, for a total of 9 mosaics (3 bands * 3 years).

Because these 9 images were normalized, their pixel values were represented in units of standard deviation from the mean pixel value (varying roughly from -3 to 3), so their data were unsuitable

for calculation of NDVI. These new 9 mosaics required denormalization before proceeding with further calculations, according to the following formula:

$$band_{mosaic} * sd(band_{ref.tile}) + mean(band_{ref.tile})$$

After denormalization, the images' pixels returned to values similar to those of their original 8-bit unsigned encoding (varying from 0 to 255). However, they retained a pixel type of 32-bit floating point due to the normalization-denormalization operation.

Next, the 9 normalized, mosaicked, and denormalized single-band raster images were composited back into 3 multispectral images for the sampled years. Figures 1a – 1c show the results of these operations as Color Infrared composites for 2020, 2016, and 2009, clipped to the extent of Beverly Hills.

NDVI can now be calculated for the three sampled years, using the normalized, mosaicked, and denormalized data from the NAIP images' NIR and Red bands.

$$NDVI = \frac{(NIR - Red)}{(NIR + Red)}$$

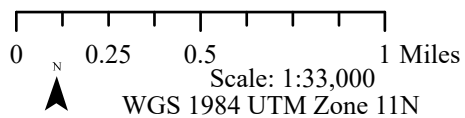
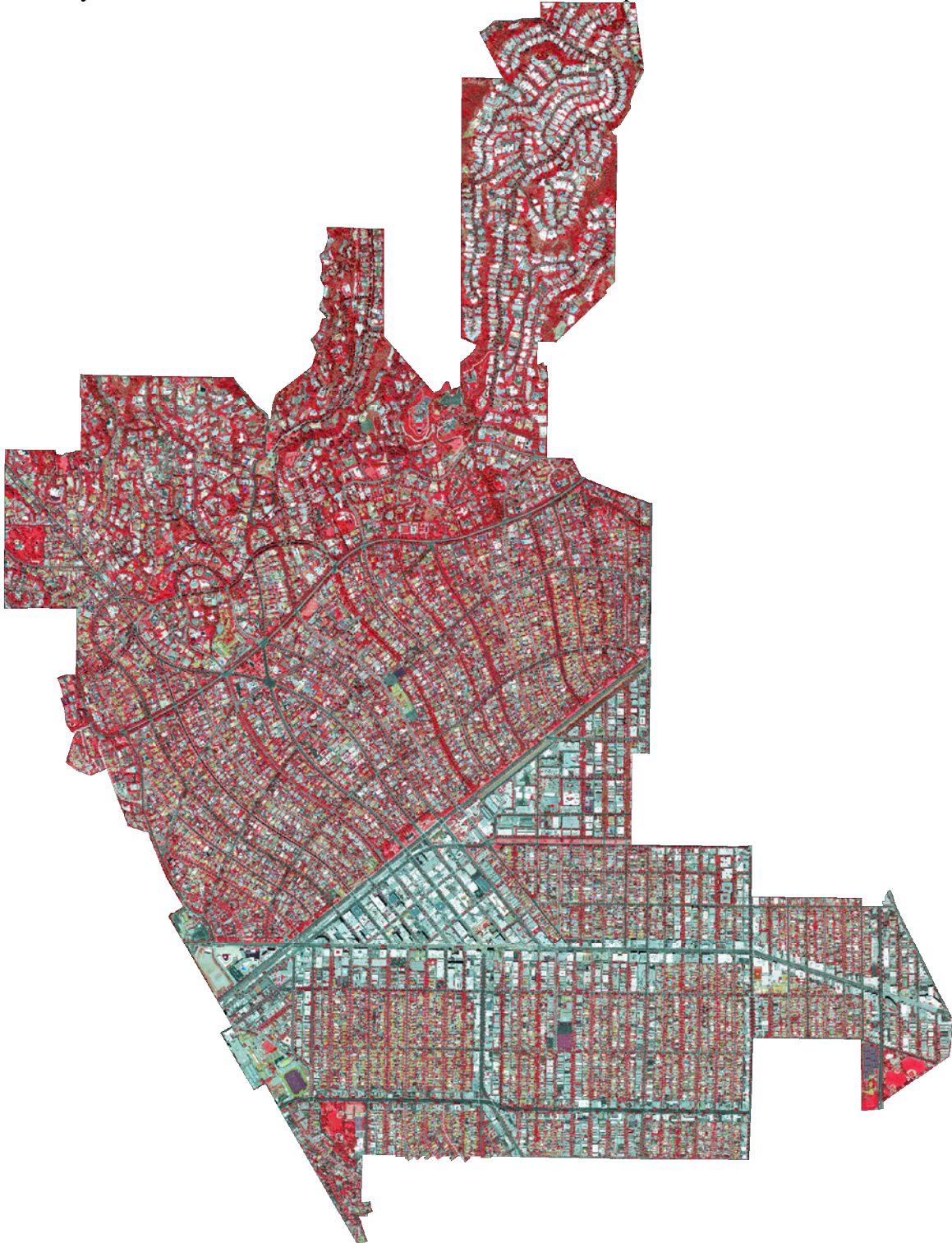
The results of the NDVI calculations for 2020, 2016, and 2009 are shown in Figures 2a – 2c.

Before proceeding with Δ NDVI analysis, I used the NDVI results to serve as an approximate image classifier to select all vegetation in Beverly Hills, by reclassifying images for each year where $NDVI > 0.1 =$ VEGETATION. This allowed for calculation of a rough estimate of “Vegetated Area” for the three sampled years. Figures 3a – 3c show the area of Beverly Hills classified as “VEGETATION” in this manner.

Next, I calculated Δ NDVI for three different periods: “Full Time Span” or Δ NDVI 2020 – 2009; “First Window of Time” or Δ NDVI 2016 – 2009; and “Second Window of Time” or Δ NDVI 2020 – 2016. The results from these calculations are shown in Figures 4a – 4c.

Figure 1a: NAIP Color-Infrared Composite, Beverly Hills, Calif. 2020
NIR, Red, and Green bands from (4) May 2020 NAIP images
individually Normalized, Mosaicked, Denormalized, and Composited

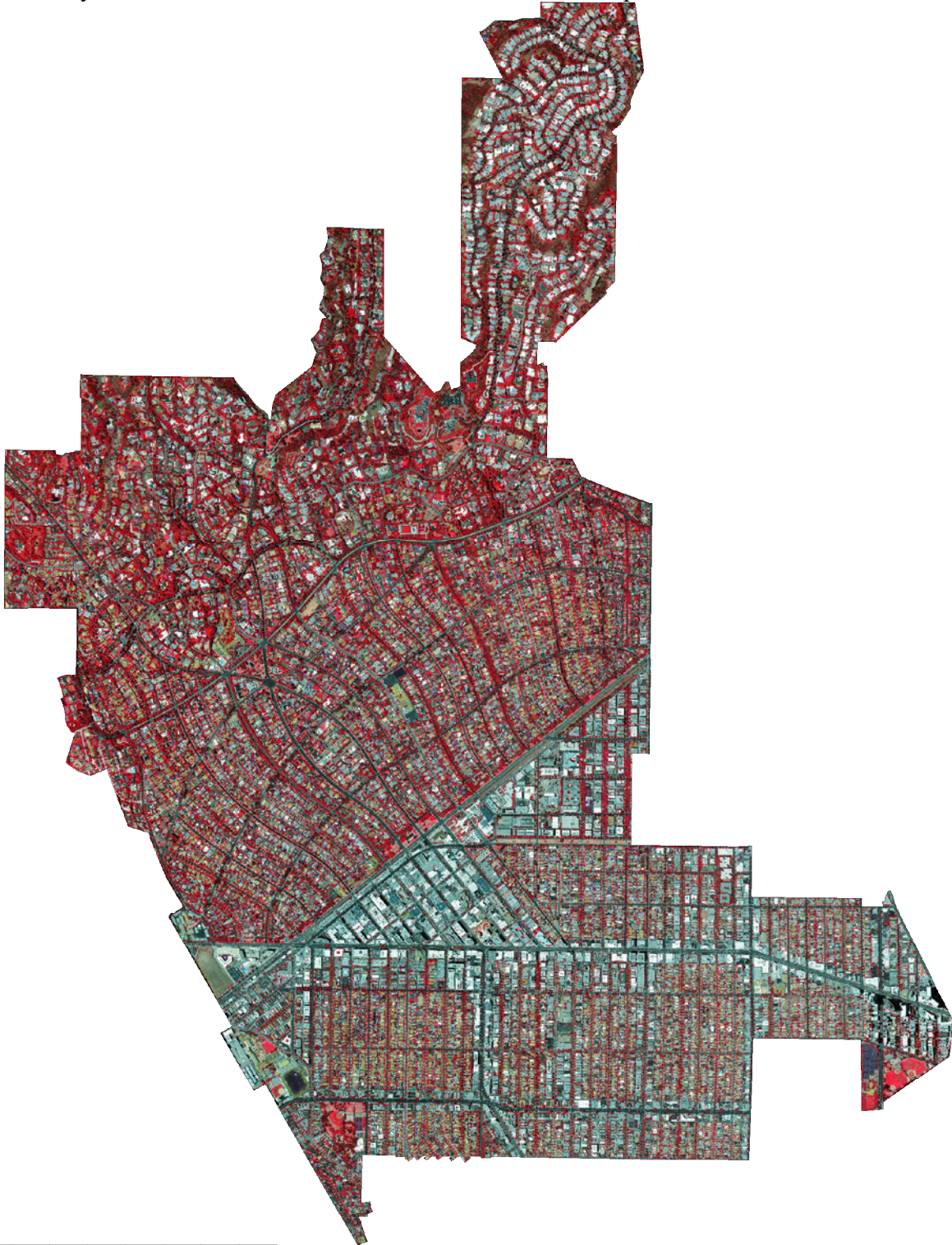
Red:NIR
Green:Red
Blue:Green



Aaron Goodman, GEOG 411: Geospatial Imagery Analysis
Prof. Greg Okin & Dr. Lincoln Pitcher
data source: USGS EROS Archive, NAIP Aerial Photography

Figure 1b: NAIP Color-Infrared Composite, Beverly Hills, Calif. 2016
NIR, Red, and Green bands from (4) July 2016 NAIP images
individually Normalized, Mosaicked, Denormalized, and Composited

Red:NIR
Green:Red
Blue:Green

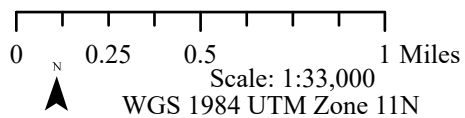
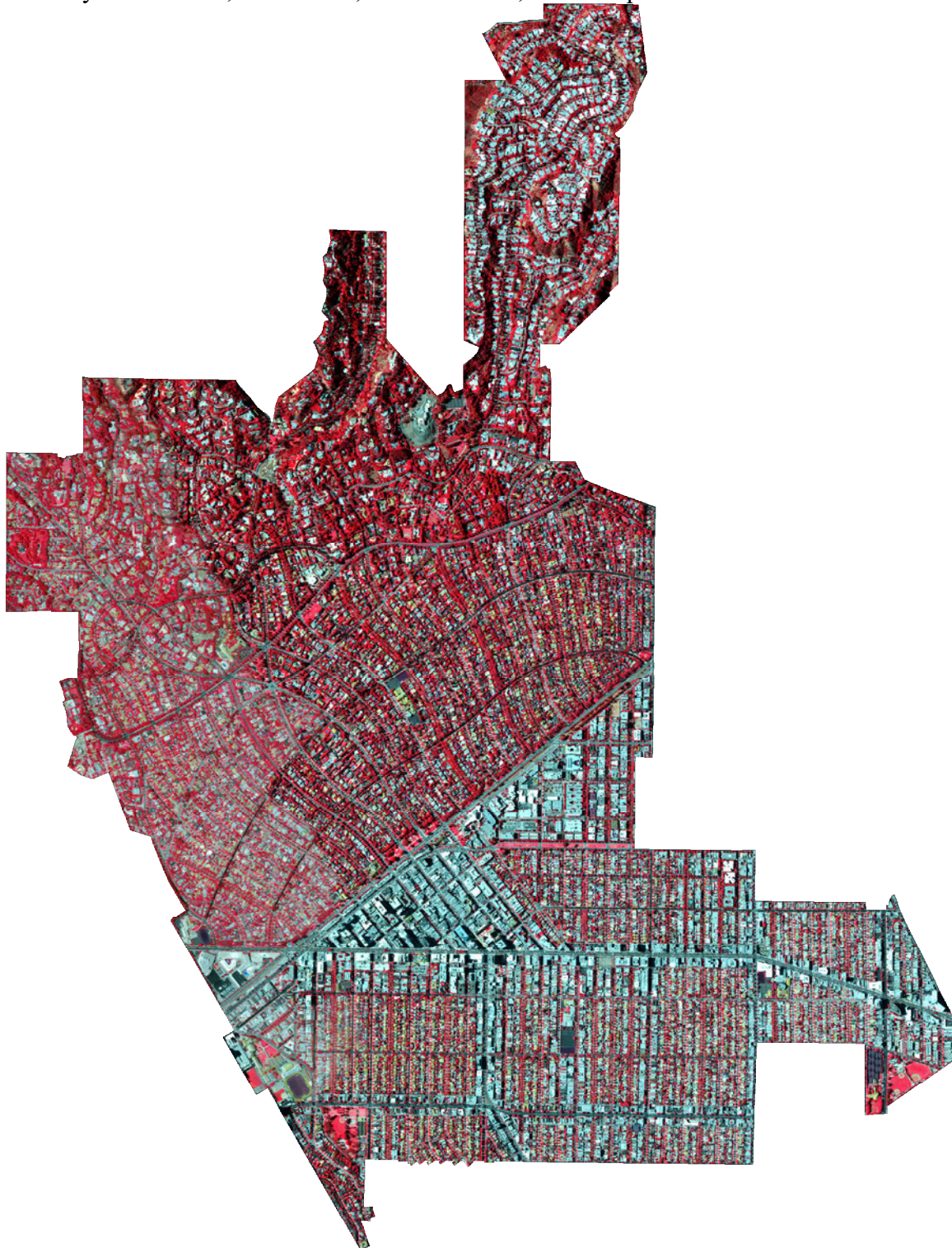


0 0.25 0.5 1 Miles
Scale: 1:33,000
WGS 1984 UTM Zone 11N

Aaron Goodman, GEOG 411: Geospatial Imagery Analysis
Prof. Greg Okin & Dr. Lincoln Pitcher
data source: USGS EROS Archive, NAIP Aerial Photography

Figure 1c: NAIP Color-Infrared Composite, Beverly Hills, Calif. 2009
NIR, Red, and Green bands from (4) June 2009 NAIP images
individually Normalized, Mosaicked, Denormalized, and Composit

Red:NIR
Green:Red
Blue:Green



Aaron Goodman, GEOG 411: Geospatial Imagery Analysis
Prof. Greg Okin & Dr. Lincoln Pitcher
data source: USGS EROS Archive, NAIP Aerial Photography

Figure 2a: NAIP-derived NDVI, Beverly Hills, Calif. 2020
NIR and Red bands from (4) May 2020 NAIP images
individually Normalized, Mosaicked, and Denormalized before calculation

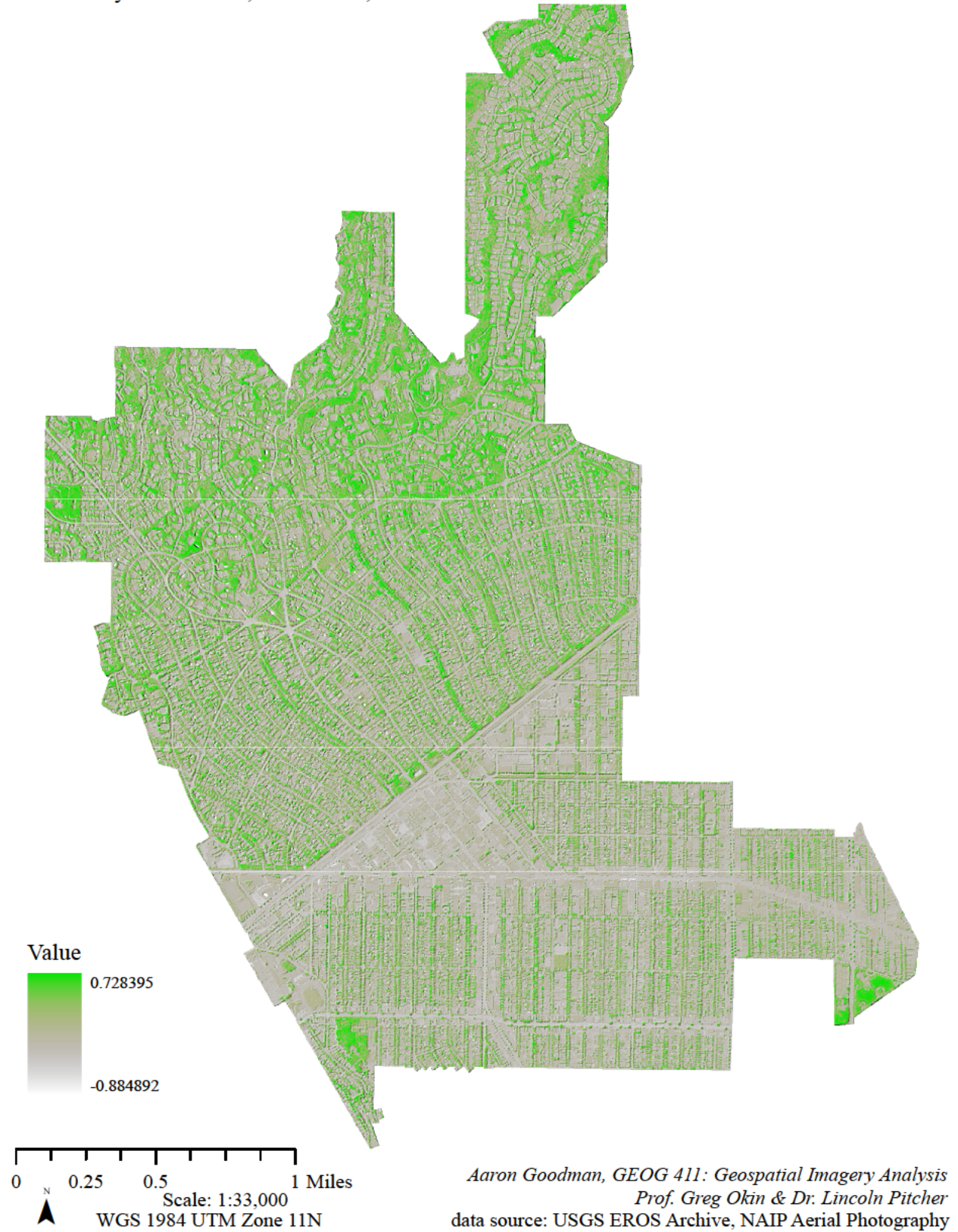


Figure 2b: NAIP-derived NDVI, Beverly Hills, Calif. 2016
NIR and Red bands from (4) July 2016 NAIP images
individually Normalized, Mosaicked, and Denormalized before calculation

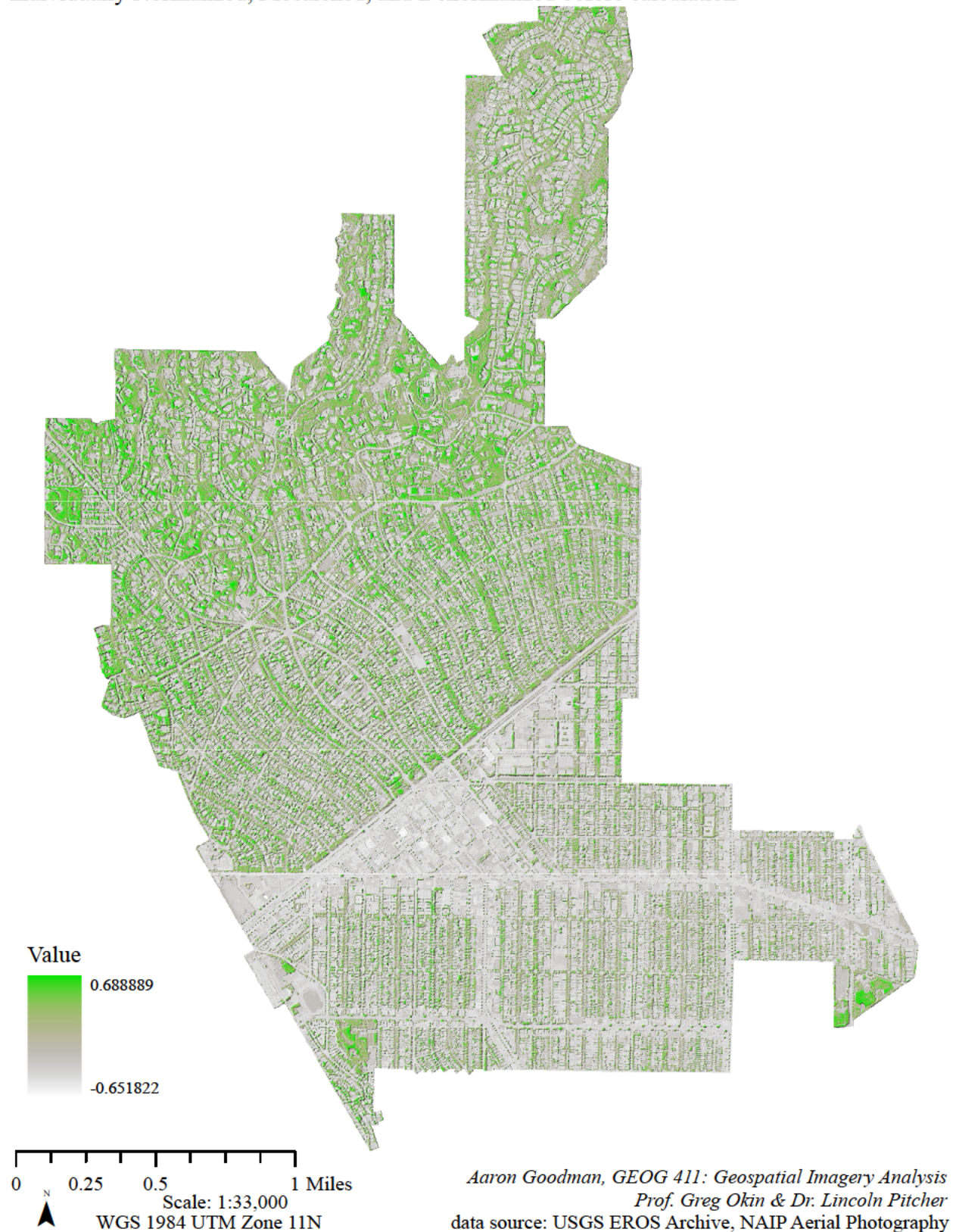


Figure 2c: NAIP-derived NDVI, Beverly Hills, Calif. 2009
NIR and Red bands from (4) June 2009 NAIP images
individually Normalized, Mosaicked, and Denormalized before calculation

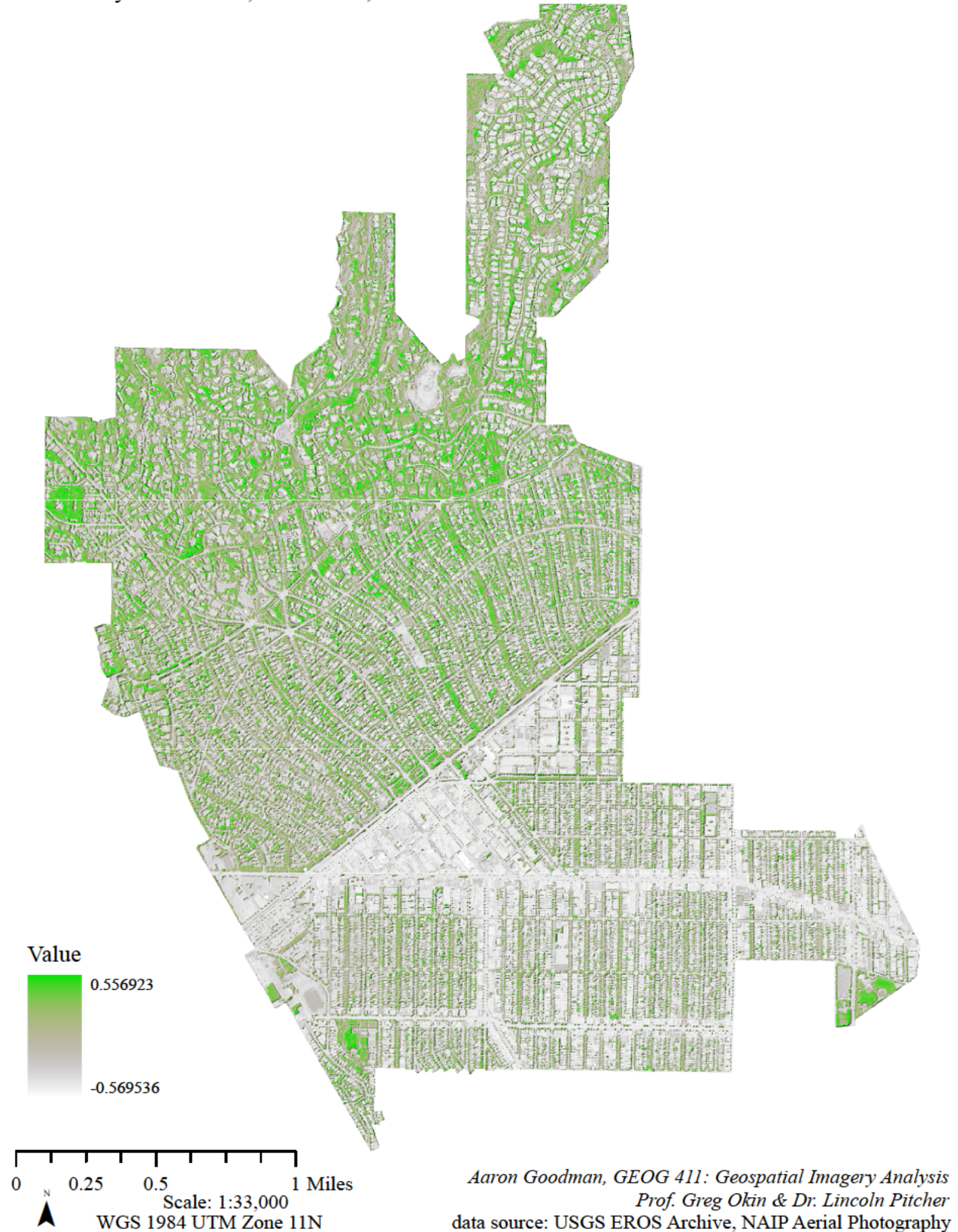


Figure 3a: NDVI > 0.1 in NAIP-derived NDVI, Beverly Hills, Calif. 2020
"Vegetation Raster" 2020

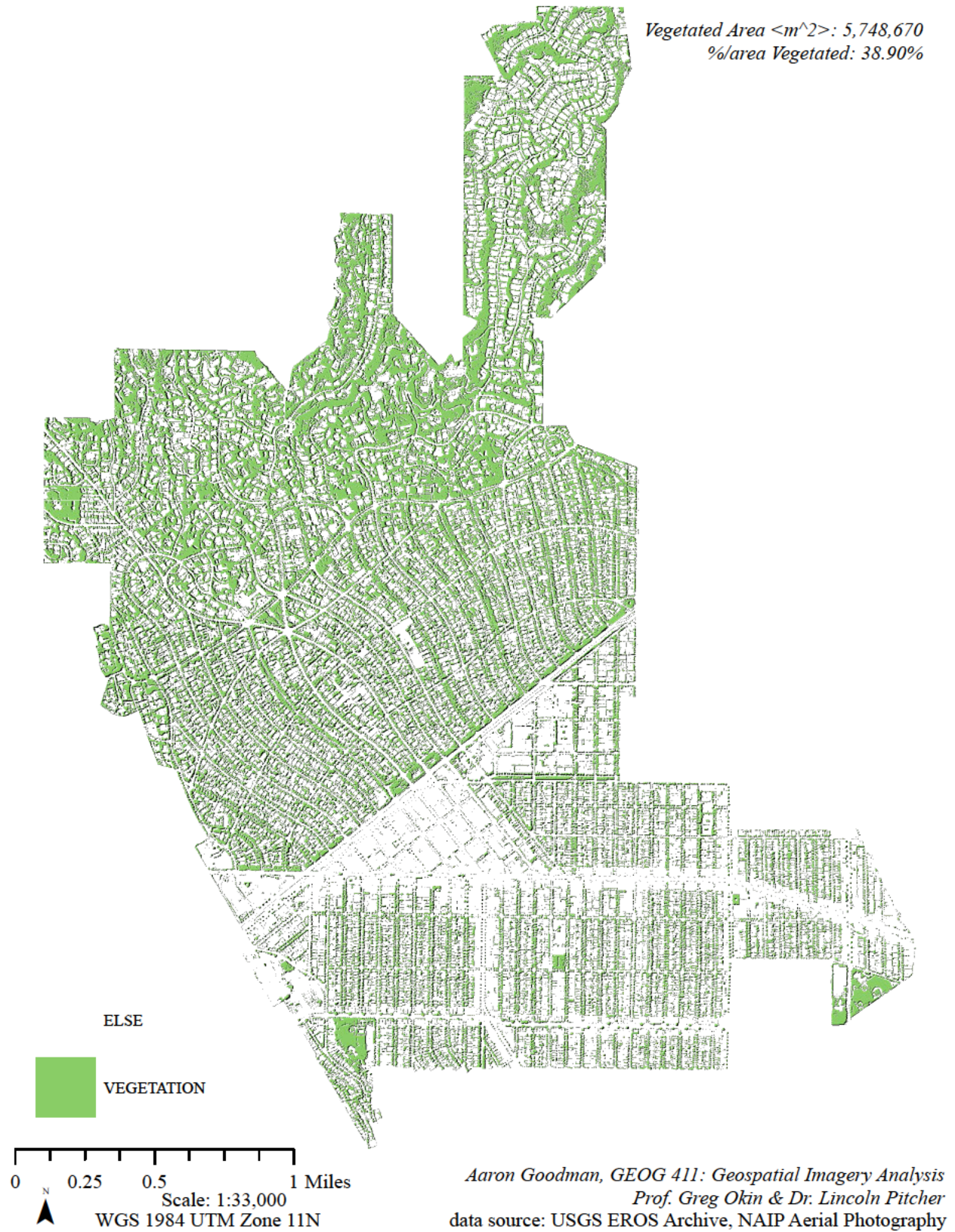


Figure 3b: NDVI > 0.1 in NAIP-derived NDVI, Beverly Hills, Calif. 2016
"Vegetation Raster" 2016

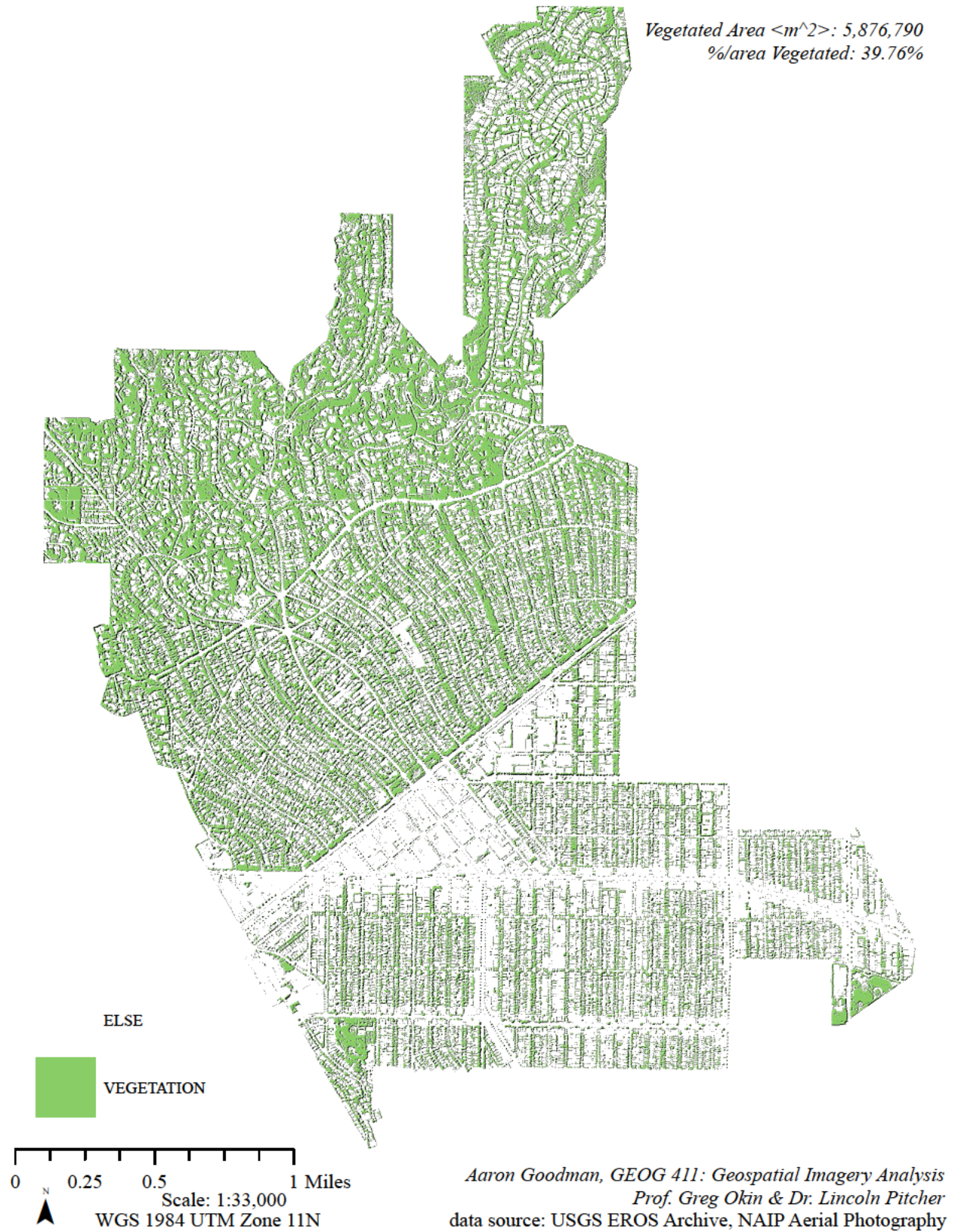


Figure 3c: NDVI > 0.1 in NAIP-derived NDVI, Beverly Hills, Calif. 2009
"Vegetation Raster" 2009

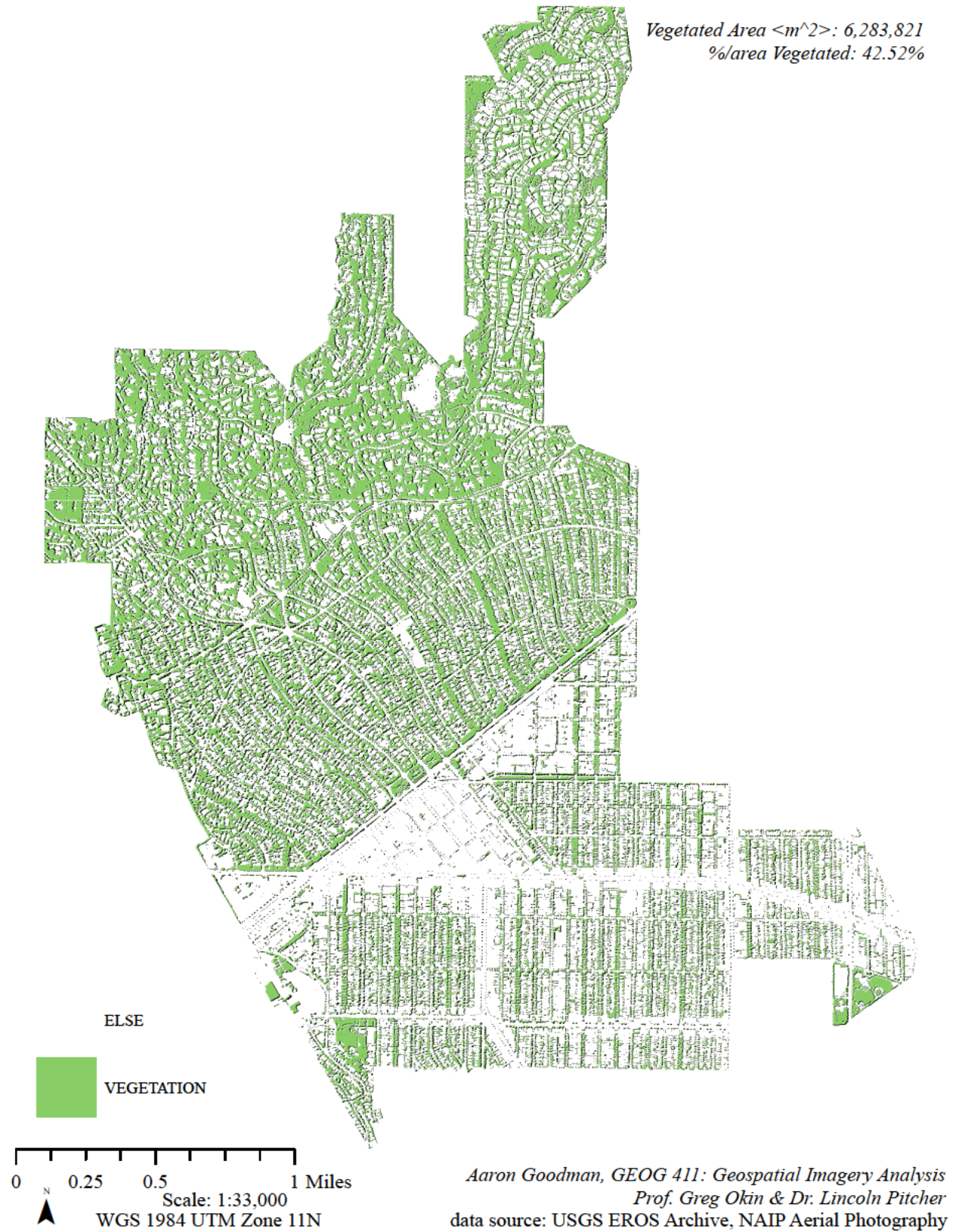


Figure 4a: Δ NDVI 2020 – 2009, Beverly Hills, Calif.
"Full Time Span"

Negative values indicate vegetation loss between sampled years; positive values indicate gain

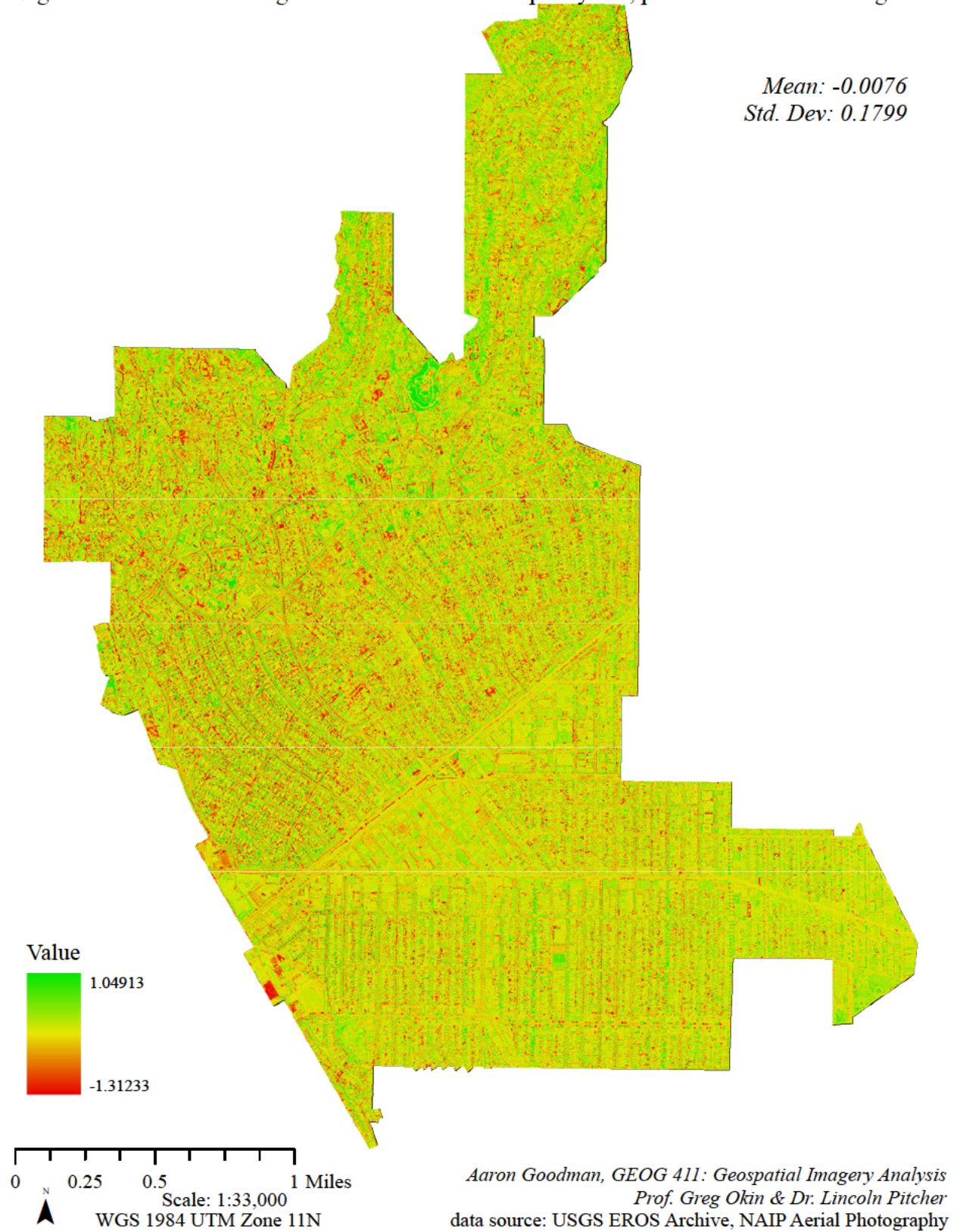


Figure 4b: Δ NDVI 2016 – 2009, Beverly Hills, Calif.

"First Window of Time"

Negative values indicate vegetation loss between sampled years; positive values indicate gain

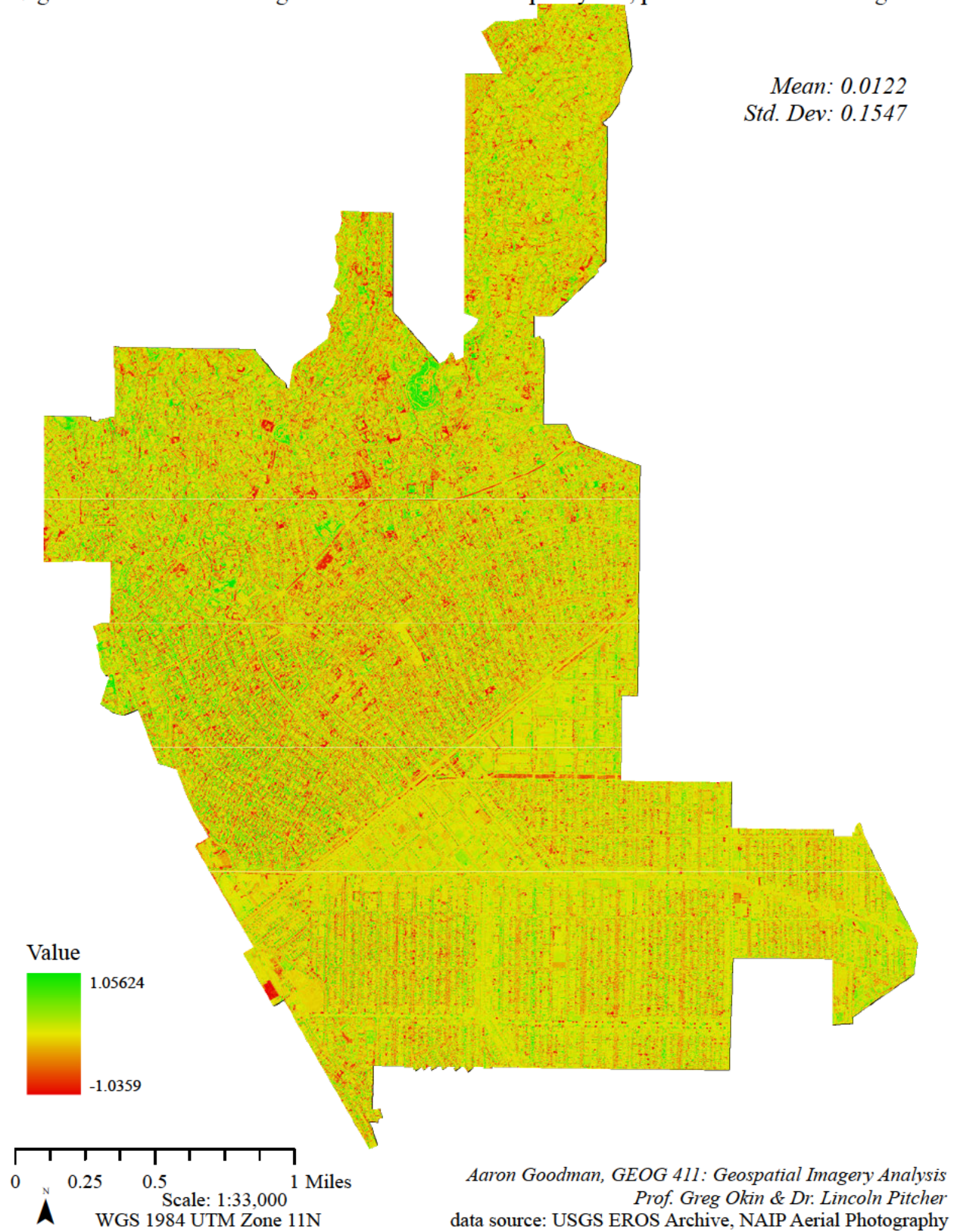
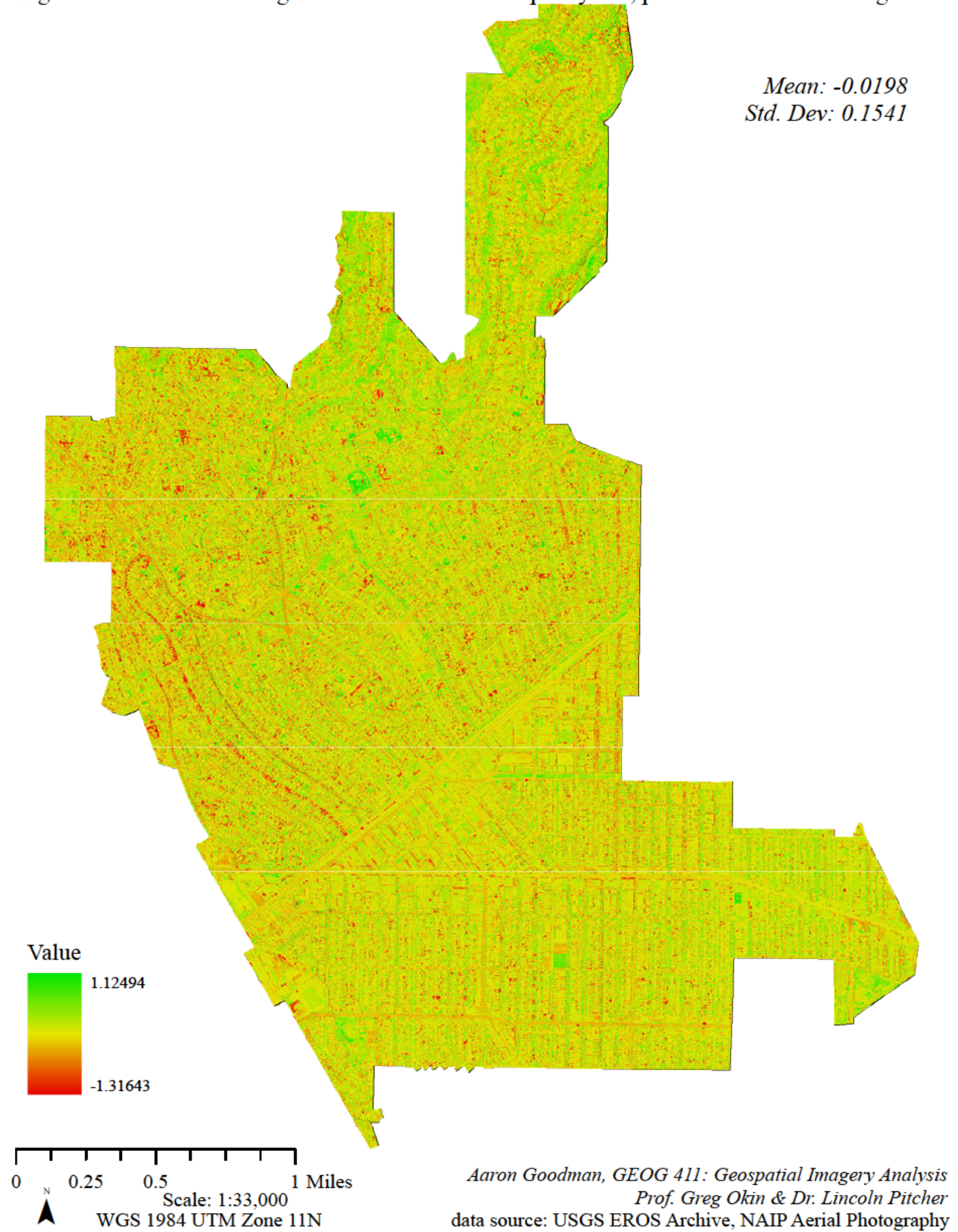


Figure 4c: Δ NDVI 2020 – 2016, Beverly Hills, Calif.

"Second Window of Time"

Negative values indicate vegetation loss between sampled years; positive values indicate gain



Next, I reclassified these three $\Delta NDVI$ images into 6 symmetrical classes centered at their mean value, according to the scheme:

- 3 = Significant Decrease = $\Delta NDVI < mean - 2sd$
- 2 = Moderate Decrease = $[mean - 2sd, mean - sd)$
- 1 = Marginal Decrease = $[mean - sd, mean)$
- 1 = Marginal Increase = $[mean, mean + sd)$
- 2 = Moderate Increase = $[mean + sd, mean + 2sd)$
- 3 = Significant Increase = $\Delta NDVI > mean + 2sd$

However, because I wanted to use a consistent classification scheme for the three different periods examined, the values for “mean” and “standard deviation” were taken from averages of those values for the three periods. Table 2 below shows how the “mean” and “sd” selected for classification varied from the real values (*avg. $\Delta NDVI$*):

Table 2: Mean and Std. Dev. $\Delta NDVI$ for three periods and Average

Difference Raster	Mean	Std. Dev.
$\Delta NDVI$ 2020 – 2009	-0.00764	0.179861
$\Delta NDVI$ 2016 – 2009	0.012207	0.154743
$\Delta NDVI$ 2020 – 2016	-0.01982	0.154104
<i>avg. $\Delta NDVI$</i>	<i>-0.00508</i>	<i>0.162903</i>

This reclassification enables quick interpretation of the arithmetic and spatial distributions of $\Delta NDVI$ values for the Full, First, and Second time spans. These 6-class raster images are shown in Figures 5a – 5c, with classes representing “Marginal” change appearing invisible to highlight regions of more notable change.

Finally, I created a “Time Series” reclassification with the 6-class $\Delta NDVI$ results, by encoding $\Delta NDVI$ 2016 – 2009 into the “one’s” place and $\Delta NDVI$ 2020 – 2016 into the “ten’s” place according to the following Raster Calculator expression:

$$36class = ([6class \Delta NDVI 2020 - 2016] * 10) + [6class \Delta NDVI 2016 - 2009]$$

Figure 5a: Reclassified Δ NDVI 2020 – 2009, Beverly Hills, Calif.
"Full Time Span"

Difference raster reclassified into 6 classes, breaks at -2sd, -sd, mean, +sd, +2sd

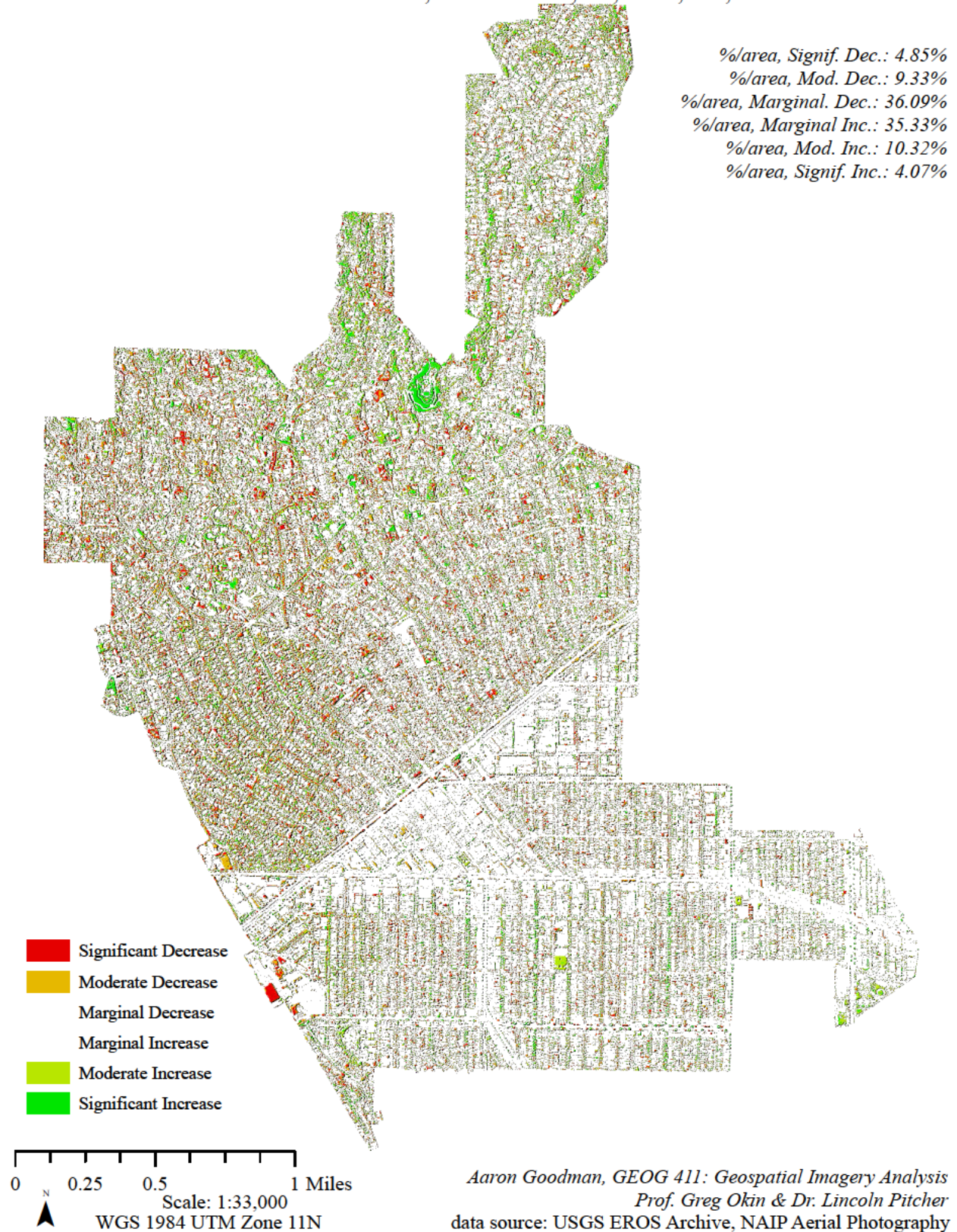


Figure 5b: Reclassified Δ NDVI 2016 – 2009, Beverly Hills, Calif.
"First Window of Time"

Difference raster reclassified into 6 classes, breaks at -2sd, -sd, mean, +sd, +2sd

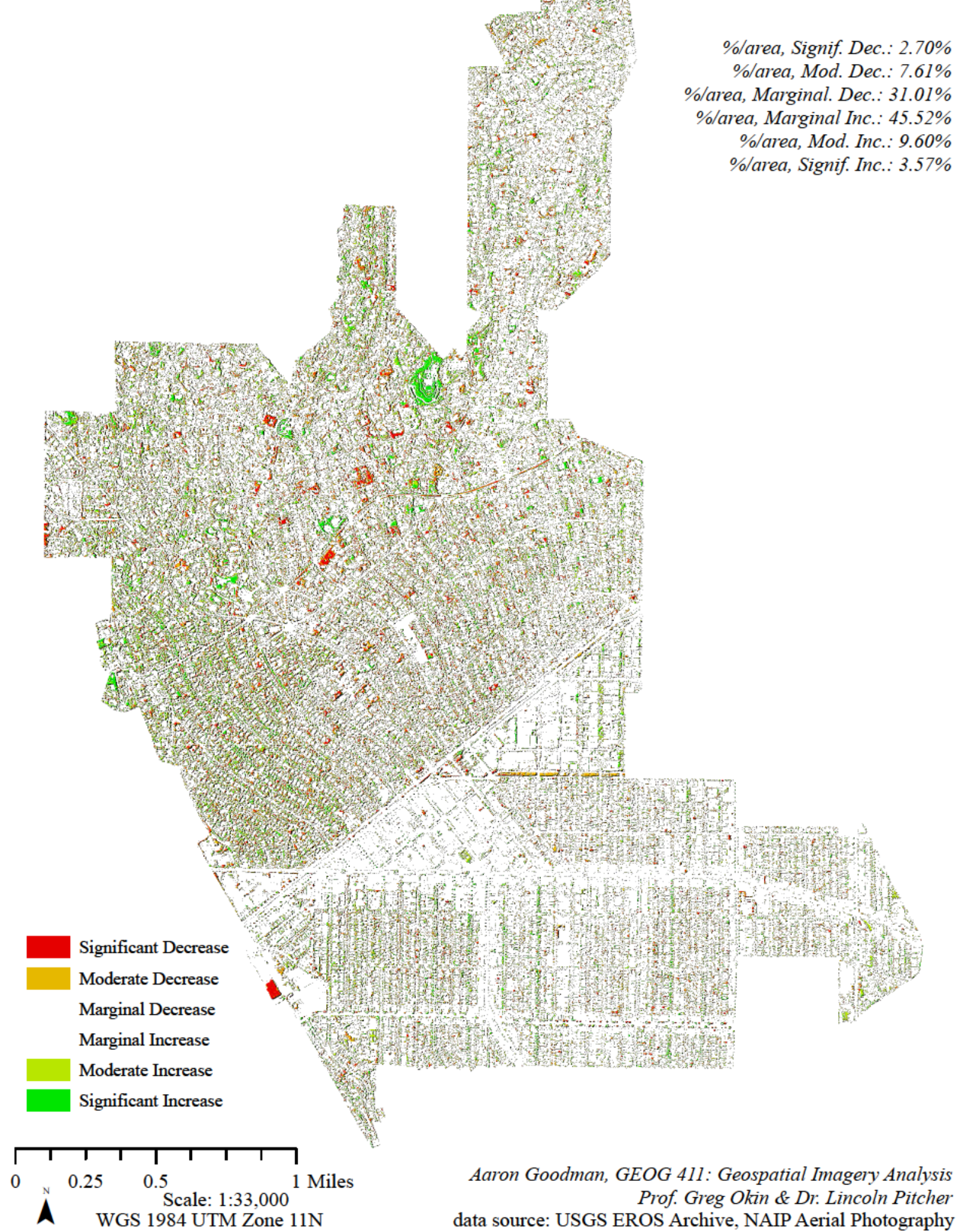
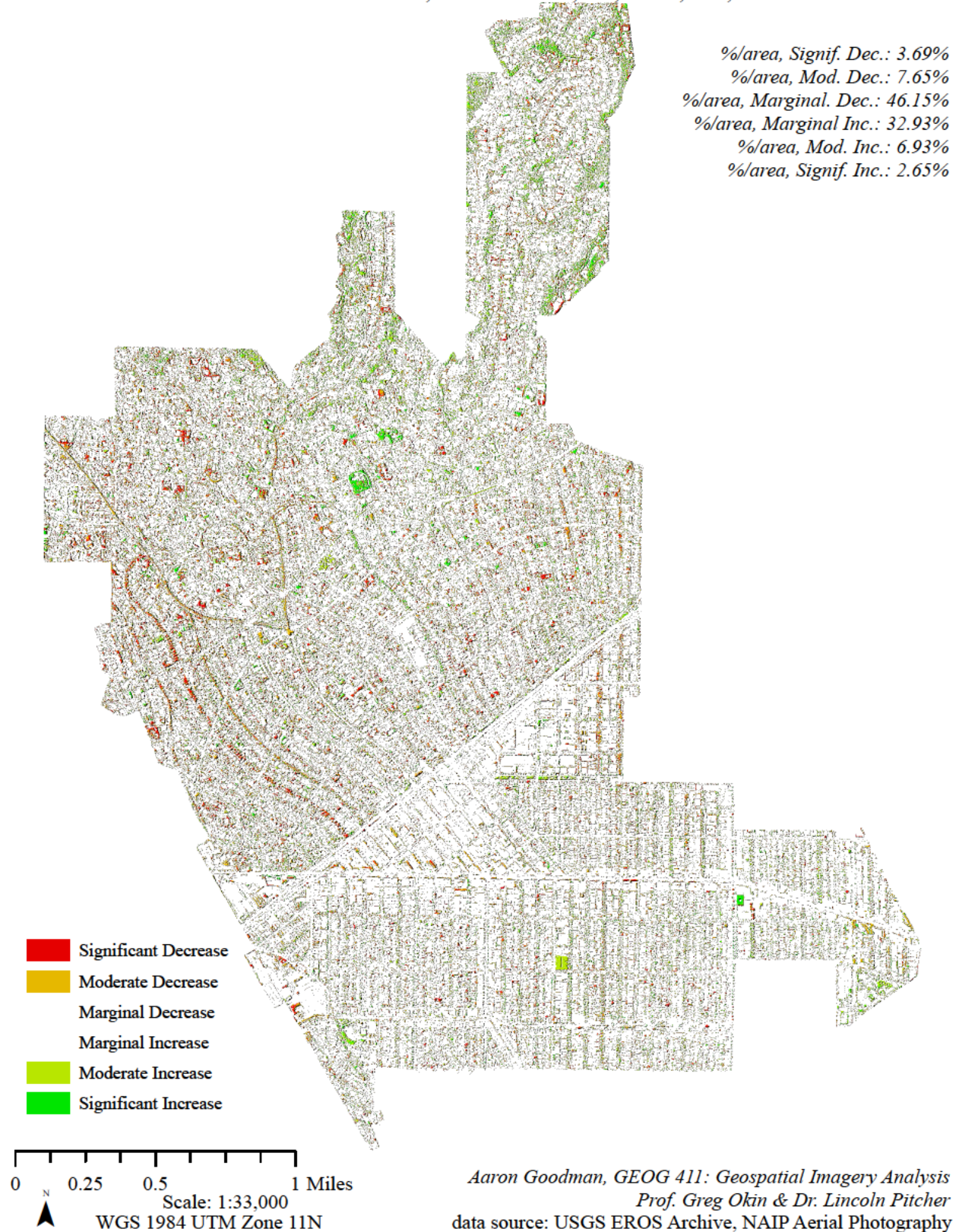


Figure 5c: Reclassified Δ NDVI 2020 – 2016, Beverly Hills, Calif.

"Second Window of Time"

Difference raster reclassified into 6 classes, breaks at -2sd, -sd, mean, +sd, +2sd



This calculation resulted in a raster image with 36 unique classes, whose values represented the pixels' Δ NDVI performance in the First Window of Time and Second Window of Time. Table 3 below outlines the matrix through which the 36 unique class values can be decoded:

Table 3: 36-class Δ NDVI Time Series class value matrix

	-3	-2	-1	+1	+2	+3	
-30	-33	-32	-31	-29	-28	-27	(decrease)
-20	-23	-22	-21	-19	-18	-17	(decrease)
-10	-13	-12	-11	-9	-8	-7	(decrease)
10	7	8	9	11	12	13	(increase)
20	17	18	19	21	22	23	(increase)
30	27	28	29	31	32	33	(increase)

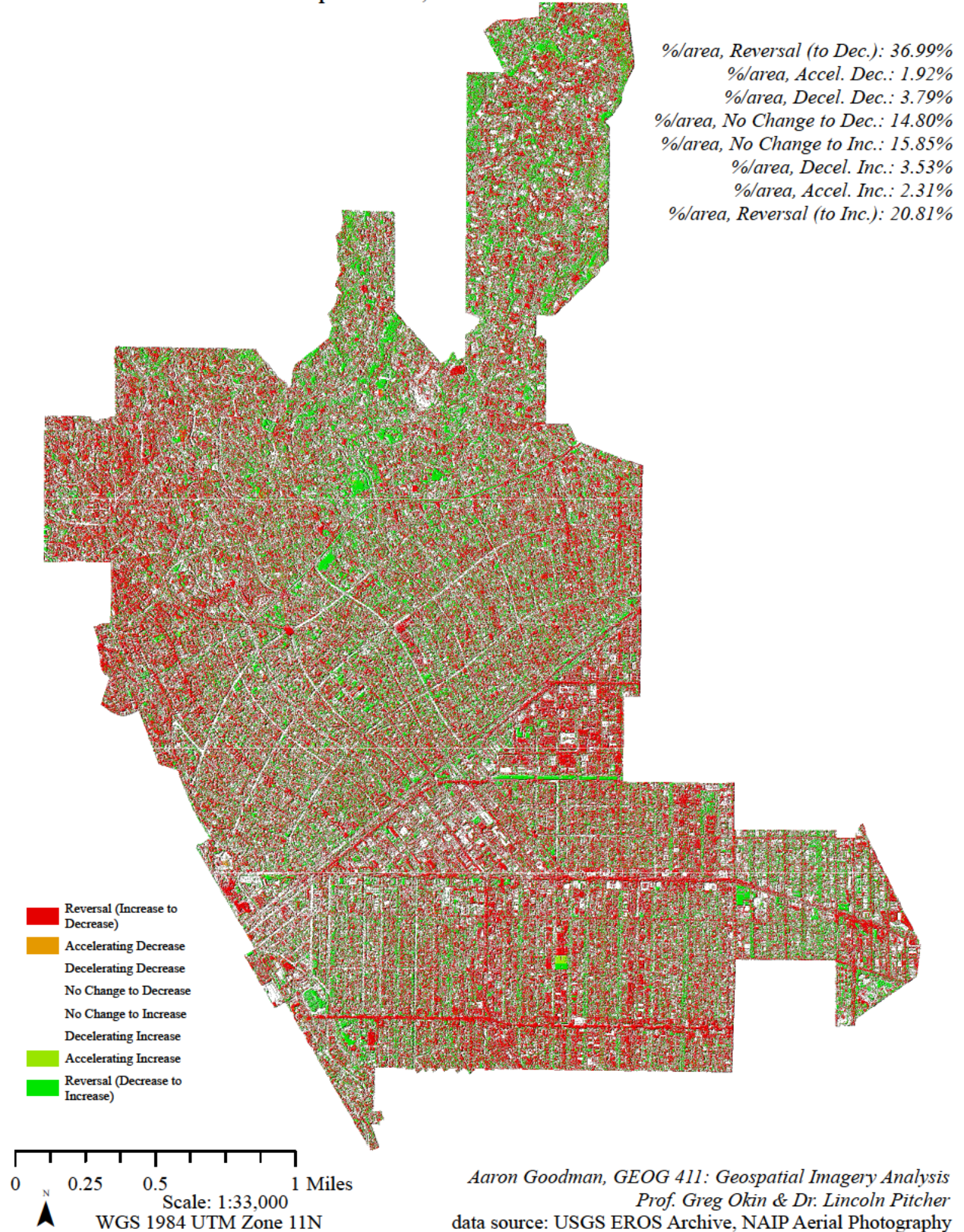
No Change
Reversal
Decelerating
Accelerating

While the 36-class Δ NDVI Time Series raster is unsuitable for presentation, one more reclassification can render it scrutable. By using the scheme:

- 8 = Reversal (Increase to Decrease) = $\{-7,-8,-9,-17,-18,-19,-27,-28,-29\}$
- 4 = Accelerating Decrease = $\{-21,-31,-32\}$
- 2 = Decelerating Decrease = $\{-12,-13,-23\}$
- 1 = No Change to Decrease = $\{-11,-22,-33\}$
- 1 = No Change to Increase = $\{11,22,33\}$
- 2 = Decelerating Increase = $\{12,13,23\}$
- 4 = Accelerating Increase = $\{21,31,32\}$
- 8 = Reversal (Decrease to Increase) = $\{7,8,9,17,18,19,27,28,29\}$

the Time Series is sorted into 8 classes which represent regions in Beverly Hills with similar rates of change for Δ NDVI across the two Windows of Time. The results of this reclassification are shown in Figure 6, with the “No Change” and “Decelerating” classes appearing invisible to highlight regions of significant $\Delta(\Delta$ NDVI).

Figure 6: Twice Reclassified, "Time-Encoded" Δ NDVI, Beverly Hills, Calif.
Change of pixel class in Reclassified NDVI Difference rasters for 2016-2009 and 2020-2016 encoded into 36 unique classes; then reclassified into 8 classes



V. Results

The Δ NDVI plots (Figures 4a – 4c) show clusters of considerable Vegetation Loss (negative Δ NDVI) in the medium- and low-density residential zones of Beverly Hills, especially in the Second Window of Time. A clearer picture is available in the 6-class reclassified Δ NDVI plots (Figures 5a – 5c), and tables of the plots’ areas by class provide quick insight into the arithmetic and spatial distribution of NDVI change through the examined time span (Tables 4a – 4c).

Table 4a: Area by Class: 6-class, reclassified Δ NDVI 2020 – 2009 “Full Span”

Class Label	Class Value	Area <m²>	Area <%>
Significant Decrease	-3	717,553	0.048549476
Moderate Decrease	-2	1,378,241	0.093251479
Marginal Decrease	-1	5,334,308	0.360918089
Marginal Increase	1	5,221,761	0.353303184
Moderate Increase	2	1,525,887	0.103241174
Significant Increase	3	602,080	0.040736598
<i>total</i>		<i>14,779,830</i>	<i>1</i>

Table 4b: Area by Class: 6-class, reclassified Δ NDVI 2016– 2009 “First Window”

Class Label	Class Value	Area <m²>	Area <%>
Significant Decrease	-3	398,557	0.026966278
Moderate Decrease	-2	1,125,088	0.076123203
Marginal Decrease	-1	4,582,696	0.310064189
Marginal Increase	1	6,728,217	0.455229661
Moderate Increase	2	1,418,165	0.095952727
Significant Increase	3	527,107	0.035663942
<i>total</i>		<i>14,779,830</i>	<i>1</i>

Table 4c: Area by Class: 6-class, reclassified Δ NDVI 2020– 2016 “Second Window”

Class Label	Class Value	Area <m²>	Area <%>
Significant Decrease	-3	545,864.4	0.036932877
Moderate Decrease	-2	1,130,657.76	0.076499665
Marginal Decrease	-1	6,821,239.32	0.461521196
Marginal Increase	1	4,866,703.92	0.329278436
Moderate Increase	2	1,023,638.76	0.06925882
Significant Increase	3	391,800.6	0.026509007
<i>total</i>		<i>14,779,904.76</i>	<i>1</i>

Table 5 similarly shows tabulated area by class for the 8-class Time Series encoded Δ NDVI plot.

Table 5: Area by Class: 8-class, Time Series encoded Δ NDVI

Class Label	Class Value	Area <m²>	Area <%>
Reversal (to Decrease)	-8	5,466,736	0.369921838
Accelerating Decrease	-4	283,076	0.019155122
Decelerating Decrease	-2	559,757	0.037877508
No Change to Decrease	-1	2,187,849	0.148046865
No Change to Increase	1	2,342,001	0.158477987
Decelerating Increase	2	522,295	0.035342538
Accelerating Increase	4	341,360	0.02309907
Reversal (to Increase)	8	3,075,010	0.208079072
<i>total</i>		<i>14,778,084</i>	<i>1</i>

Tables 4a – 4c complement the various Δ NDVI plots to illustrate a general trend of vegetation reduction in Beverly Hills, especially as the First Window of Time rolled into the Second. In particular, Δ NDVI 2016– 2009 “First Window” exhibits 46% of the city’s land marginally increasing in vegetation cover and 31% of land marginally decreasing, while Δ NDVI

2020– 2016 “Second Window” sees a switch to 46% marginally decreasing and 33% marginally increasing. The “First Window” also saw 2.7% of Beverly Hills land significantly decreasing in vegetation cover and 3.6% significantly increasing, while the “Second Window” saw 3.7% significantly decreasing and 2.7% significantly increasing.

Table 5 further supports these observations, by showing that the majority of Beverly Hills land (37% of the city’s total area) saw a reversal in vegetation change between the two time periods, where vegetation cover increased 2009 – 2016 and decreased 2016 – 2020. This portion of the city’s land is considerably greater than the next largest class (21%) which saw a reversal in the opposite direction, where vegetation cover decreased 2009 – 2016 and increased 2016 – 2020.

The most straightforward results come from estimates of “Vegetated Area” in Figures 3a – 3c, also shown in Tables 6a – 6c below.

Table 6a: Area by Class: “Vegetation Raster” 2020 (NDVI > 0.1 = VEGETATION)

Class Label	Class Value	Area <m²>	Area <%>
ELSE	0	9,031,234.68	0.611048232
VEGETATION	1	5,748,670.08	0.388951768
<i>total</i>		<i>14,779,904.76</i>	<i>1</i>

Table 6b: Area by Class: “Vegetation Raster” 2016 (NDVI > 0.1 = VEGETATION)

Class Label	Class Value	Area <m²>	Area <%>
ELSE	0	8,903,114.64	0.602379703
VEGETATION	1	5,876,790.12	0.397620297
<i>total</i>		<i>14,779,904.76</i>	<i>1</i>

Table 6c: Area by Class: "Vegetation Raster" 2009 (NDVI > 0.1 = VEGETATION)

Class Label	Class Value	Area <m ² >	Area <%>
ELSE	0	8,496,009	0.574838073
VEGETATION	1	6,283,821	0.425161927
<i>total</i>		14,779,830	1

These estimates, derived from the rough NDVI > 0.1 classification that selected vegetated land cover, show total vegetation cover reduction of 535,151 m² from 2009 to 2020, or an 8.516% reduction in vegetation cover. 407,031 m² of vegetation were removed between 2009 and 2016 for a 6.926% reduction in vegetation cover, and 128,120 m² were removed between 2016 and 2020 for a 2.180% reduction in vegetation cover (6.284 km² to 5.877 km² to 5.749 km²). This general reduction in "Vegetated Area" (from 43% of Beverly Hills to 39%) is evident in the NDVI > 0.1 plots of Figures 3a – 3c, which show vegetation density decreasing in residential areas across the examined time periods.

This change in Vegetated Area is converted into an estimate of Annual Landscape Water Use according to the framework set forward by the U.S. Department of Energy's Federal Energy Management Program in their "Guidelines for Estimating Unmetered Landscaping Water Use" (U.S. Department of Energy 2010). One of the methods of estimation presented in this document is that of the evapotranspiration (ET) method, which provides a formula with which users can roughly estimate Annual Landscape Water Use with user-provided Irrigation Area, an Annual Irrigation Factor specific to the type of vegetation cover and regional climate of interest, and a rough estimate of Irrigation System Efficiency. Annual Irrigation Factors for various types of vegetation and regions are supplied in the document, along with guidelines for assessing the efficiency of examined irrigation systems.

The following Annual Irrigation Factors are provided for Los Angeles (Table 7):

Table 7: Annual Irrigation Factors for Los Angeles, as supplied by U.S. D.o.E.

Landscape Type	Annual Irrigation Factor
Cool-season turf-grass	20.72
Warm-season turf-grass	14.64
High-water req. low density-protected microclimate	10.59
High-water req. avg. density-open microclimate	20.94
High-water req. high density-intense exposure	36.62
Moderate-water req. low density-protected microclimate	5.5
Moderate-water req. avg. density-open microclimate	11.75
Moderate-water req. high density-intense exposure	20.14
Low-water req. low density-protected microclimate	1.09
Low-water req. avg. density-open microclimate	1.98
Low-water req. high density-intense exposure	6.81
<i>avg.</i>	<i>13.70727273</i>

Due to lack of a more sophisticated model of vegetation cover types, I chose to use a rough average of Los Angeles’s Annual Irrigation Factors for this calculation: an even 14. I assumed an average Irrigation System Efficiency of 80% according to the Department of Energy’s guidelines, as well as following suit from prior examinations of irrigation requirements in Arizona (Saher, et al. 2022). Next, I simply had to convert my Vegetated Areas into square feet (Table 8) to be able to use the provided ET method formula to estimate Annual Landscape Water Use (ALWU):

$$ALWU \left(\frac{gal}{yr} \right) = \frac{\left(Annual\ Irrigation\ Factor \left(\frac{gal}{ft^2 * yr} \right) * Irrigation\ Area\ (ft^2) \right)}{Irrigation\ System\ Efficiency}$$

Table 8: "Vegetated Area" by Year, m² and ft²

Year	Area <m ² >	Area <ft ² >
2020	5,748,670.08	61,878,169.8
2016	5,876,790.12	63,257,242.4
2009	6,283,821	67,638,486

$$ALWU \left(\frac{gal}{yr} \right) = \frac{(14 * Irrigation Area)}{0.8}$$

The results of these calculations are listed below in Table 9:

Table 9: Annual Landscape Water Use by Year, gal/yr

Year	ALWU <gal/yr>	ΔALWU <gal/yr>
2020	1,082,867,971.5	↑ -24,133,770.5 (-100,805,533.5 total)
2016	1,107,001,742	↑ -76,671,763
2009	1,183,673,505	↑

While the generation of these estimates was not the most rigorous, the downward trend observed in Beverly Hills' Annual Landscape Water Use (ALWU) between 2009 and 2020 does resonate with our findings in the city's vegetation reduction. According to these estimates, Beverly Hills' vegetation required about 101 million less gallons of water per year in 2020 than the city required in 2009 (1.184 billion gallons of water per year in 2009 to 1.083 billion gallons of water per year in 2020). This accounts for an 8.516% reduction in Annual Landscape Water Use over the course of 11 years.

VI. Discussion

There are a number of potential sources of error and uncertainty in this study, stemming from the low temporal resolution of NAIP imagery, as well as from the lack of rigor in this model's identification of vegetation cover and type.

The sampled NAIP images exhibited remarkably different solar angles due to their collection at different times of the year (May 2020, July 2016, and June 2009), and this inconsistency may have introduced uncertainty in the model's interpretation of the images' spectral distributions. Beyond this, the use of scenes from different seasons (or times of the season) may have eliminated some accuracy in the assessment of each year's vegetation loss or growth.

Because the estimates for Annual Landscape Water Use (ALWU) presented in this study were the result of several rough approximations (no delineation of distinct vegetation types meant assuming one averaged Annual Irrigation Factor for all of Beverly Hills' vegetation; and 80% Irrigation Efficient was assumed for the entire city), the report that 100 million less gallons of water per year were required for 2020's vegetation than that of 2009, must come with this important caveat.

VII. Conclusion

This study aims to assess Beverly Hills' water savings over 11 years using a rudimentary estimation of the city's vegetation cover, as it can be measured from NAIP aerial imagery via NDVI analysis. While this research would reduce error and greatly benefit from a more robust analysis of vegetation types, the rough illustration of vegetation loss captured here does reflect the trends expected of a city adopting Xeriscaping practices. Through Beverly Hills' reduction of vegetation land cover by 535,151 m² or 8.516% from 2009 to 2020, this study estimates that the city saves approximately 100 million gallons of water annually.

VIII. References

Texts

1. Kahrl, William L. 1982. *Water and power: The conflict over Los Angeles water supply in the Owens Valley*. Univ of California Press, 1982.
2. United States Department of Energy. 2010. "Guidelines for Estimating Unmetered Landscaping Water Use" Federal Energy Management Program.
<https://www.energy.gov/femp/articles/guidelines-estimating-unmetered-landscaping-water-use>
3. Saher, Rubab, Ariane Middel, Haroon Stephen, and Sajjad Ahmad. 2022. "Assessing the Microclimate Effects and Irrigation Water Requirements of Mesic, Oasis, and Xeric Landscapes" *Hydrology* 9, no. 6: 104. <https://doi.org/10.3390/hydrology9060104>
4. Ismaeil, Esam M. H., and Abu Elnasr E. Sobaih. 2022. "Assessing Xeriscaping as a Retrofit Sustainable Water Consumption Approach for a Desert University Campus" *Water* 14, no. 11: 1681. <https://doi.org/10.3390/w14111681>
5. Li, Zhao-Liang, Ronglin Tang, Zhengming Wan, Yuyun Bi, Chenghu Zhou, Bohui Tang, Guangjian Yan, and Xiaoyu Zhang. 2009. "A Review of Current Methodologies for Regional Evapotranspiration Estimation from Remotely Sensed Data" *Sensors* 9, no. 5: 3801-3853. <https://doi.org/10.3390/s90503801>
6. Bhattarai, Nishan, and Pradeep Wagle. 2021. "Recent Advances in Remote Sensing of Evapotranspiration" *Remote Sensing* 13, no. 21: 4260.
<https://doi.org/10.3390/rs13214260>
7. Stephen, Haroon. 2018. "Trend Analysis of Las Vegas Land Cover and Temperature Using Remote Sensing" *Land* 7, no. 4: 135. <https://doi.org/10.3390/land7040135>

8. Winseck, Kevin. 2023. "Heat Islands in a Sea of Water Conservation: Heat Costs of Turf Replacement Programs". Available at SSRN: <https://ssrn.com/abstract=4378199> or <http://dx.doi.org/10.2139/ssrn.4378199>

NAIP Scenes

1. [M_3411862_NW_11_060_20200505 - EarthExplorer](#)
2. [M_3411862_SW_11_060_20200505 - EarthExplorer](#)
3. [M_3411861_NE_11_060_20200515 - EarthExplorer](#)
4. [M_3411861_SE_11_060_20200515 - EarthExplorer](#)
5. [M_3411862_NW_11_H_20160710 - EarthExplorer](#)
6. [M_3411862_SW_11_H_20160710 - EarthExplorer](#)
7. [M_3411861_NE_11_H_20160711 - EarthExplorer](#)
8. [M_3411861_SE_11_H_20160711 - EarthExplorer](#)
9. [M_3411862_NW_11_1_20090626 - EarthExplorer](#)
10. [M_3411862_SW_11_1_20090626 - EarthExplorer](#)
11. [M_3411861_NE_11_1_20090626 - EarthExplorer](#)
12. [M_3411861_SE_11_1_20090626 - EarthExplorer](#)